Dynamics inside Ion Pairs. NMR Studies of a [1-Silylallyl]lithium with a Pendant Ligand: [1-[[[Bis(2-methoxyethyl)amino]methyl]dimethylsilyl]allyl]-lithium

Gideon Fraenkel* and Jose A. Cabral

Contribution from the Department of Chemistry, The Ohio State University, Columbus, Ohio 43210-1173. *Received August 10, 1992*

Abstract: Proton and ^{13}C NMR studies of the title compound, **4**, in THF-d_8 and toluene-d_8 show it to exist as an equilibrium mixture of *endo*-silyl and *exo*-silyl species in which lithium is tridentately complexed to the pendant ligand and the whole coordination moiety is bent over the plane of the allyl anion. NMR line-shape analysis, using several different resonances, establishes the $\Delta H^{\ddagger}$ for rotation around the SiC_1–C_2 allyl bond to be 16 ± 0.5 kcal/mol. Further, for rotation of coordinated Li^+ around the Si–C_1 (allyl) bond $dH^{\ddagger}$ is 7 ± 0.4 kcal/mol. This value is similar to the activation parameters for reorientation of ions within ion pairs of (silylallyl)lithiums investigated previously.

Allyllithium is perhaps the simplest conjugated carbanionic[1] species and has been extensively studied spectroscopically[2,3] by NMR and UV, crystallographically,[4] and theoretically by calculations[5] as well as for its extensive chemistry.[6]

The stabilization of carbanionic substances by α-silyl substituent(s) is well-known but not understood.[7] Silylallyl lithiums have attracted considerable attention for their chemical virtues[8-10] as well as their physical structures and unusual dynamic behavior.[11-13] For example, electrophiles tend to react at C_3 of **1** giving

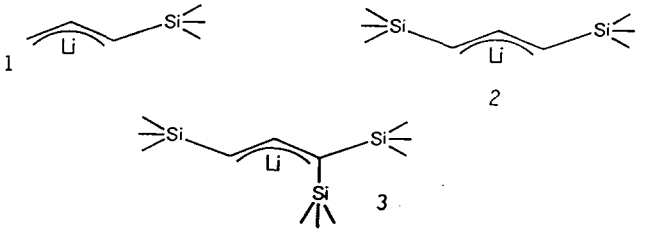

trans product,[8-10] which implicates but does not establish the exo structure shown, **1**. This was later confirmed with NMR methods. In fact, NMR established that a trimethylsilyl group at a terminal carbon on allyllithium preferentially occupies the exo site, as shown in partial structures **1–3**.[11-13] NMR of **2**·TMEDA solutions[12] as well as X-ray crystallography of monomeric **2**·TMEDA[14] show that complexed Li^+ lies on one side of the allyl plane and is unsymmetrically sited with respect to this allyl loop. Reorientation of coordinated Li^+ is slow at 150 K with a mean lifetime of ca. 2 s. The accompanying value for $\Delta H^{\ddagger}$ is 7 kcal/mol. Similar effects were observed for **1** complexed to pentamethyldiethylenetriamine[11] and for (1,1,3,3-tetramethylallyl)lithium·TMEDA.[15] The nature of this reorientation process is not yet clear.

This paper deals with the behavior of the title compound, **4**, a (silylallyl)lithium with a pendant potential ligand, [bis(2-methoxyethyl)amino]methyl, attached to silicon, first reported by Chan and Horvath.[16] These authors proposed that if **4** assumes

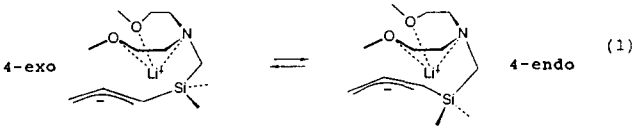

the fully folded, internally complexed conformation, then perhaps proximity of Li^+ to C_1 would favor reaction of electrophiles at C_1 instead of the usual result for **1**, exclusive reaction at C_3. The experiment was tried; reaction took place at C_1 and C_3 at similar rates.[16]

(1) Wardell, J. L. *Comprehensive Organometallic Chemistry*; Wilkinson, G., Stone, F. G. H., Abel, E. W., Eds.; Pergamon Press: Oxford, 1982; Vol. 7, p 97.

(2) (a) West, P.; Purmort, J. I.; McKinley, S. V. *J. Am. Chem. Soc.* **1968**, *90*, 797. (b) O'Brian, D. H.; Hart, A. J.; Russell, C. R. *J. Am. Chem. Soc.* **1975**, *97*, 4410. (c) Benn, R.; Rufinska, A. *J. Organomet. Chem.* **1982**, *239*, C19.

(3) (a) Bates, R. B.; Beavers, W. A. *J. Am. Chem. Soc.* **1974**, *96*, 5001. (b) Dolinskaya, E. R.; Poddabnyi, I. Ya; Tseretech, I. Yu. *Dokl. Akad. Nauk SSSR* **1970**, *191*, 802. (c) Thompson, T. B.; Ford, W. T. *J. Am. Chem. Soc.* **1979**, *101*, 5459.

(4) (a) Koster, H.; Weiss, E. *Chem. Ber.* **1982**, *115*, 3422. (b) Schumann, U.; Weiss, E.; Dietrich, H.; Mahdi, W. *J. Organomet. Chem.* **1987**, *322*, 299. (c) Sebastian, J. F.; Grunwell, J. R.; Hsu, B. *J. Organomet. Chem.* **1974**, *78*, C1. (d) Boche, G.; Etzrodt, H.; Marsh, M.; Massa, H.; Baum, G.; Dietrich, H.; Mahdi, W. *Angew. Chem.* **1986**, *98*, 84.

(5) (a) Erusalimski, C. B.; Kormer, V. H. *Zh. Org. Khim.* **1984**, *20*, 2028. (b) Tidwell, E. R.; Russell, B. R. *J. Organomet. Chem.* **1974**, *80*, 175. (c) Boche, G.; Decher, G. *J. Organomet. Chem.* **1983**, *259*, 31. (d) Clarke, T.; Jemmis, E. D.; Schleyer, P. v. R.; Binkley, J. S.; Pople, J. A. *J. Organomet. Chem.* **1978**, *150*, 1. (e) Clarke, T.; Rhode, C.; Schleyer, P. v. R. *Organometallics* **1983**, *2*, 1344. (f) Bushby, R. J.; Tytho, M. P. *J. Organomet. Chem.* **1984**, *270*, 265.

(6) (a) Seyferth, D.; Jula, T. P. *J. Organomet. Chem.* **1967**, *8*, C13. (b) Schlosser, M.; Stahle, N. *Angew. Chem.* **1980**, *92*, 477. (c) Stahle, M.; Schlosser, M. *J. Organomet. Chem.* **1981**, *220*, 277. (d) Neugebauer, W.; Schleyer, P. v. R. *Ibid* **1980**, *198*, C1. (e) Brownstein, S.; Bywater, S.; Worsfold, D. J. *Ibid.* **1980**, *199*, 1.

(7) See: Schleyer, P. v. R.; Clark, T.; Kos, A. J.; Spitznagel, G. W.; Rohde, C.; Arad, D.; Houk, K. W.; Rondan, N. G. *J. Am. Chem. Soc.* **1984**, *106*, 6472.

(8) (a) Corriu, R. J. P.; Masse, J. *J. Organomet. Chem.* **1973**, *57*, C5. (b) Corriu, R. J. P.; Masse, J.; Samate, D. *J. Organomet. Chem.* **1975**, *93*, 71. (c) Corriu, R. J. P.; Lanneau, G. F.; Ledereq, D.; Samate, D. *J. Organomet. Chem.* **1978**, *144*, 155. (d) Furuya, N.; Sukawa, T. *J. Organomet. Chem.* **1975**, *96*, C1. (e) Matsumoto, H.; Yako, T.; Nagashimi, S.; Motega, T.; Nagai, Y. *J. Organomet. Chem.* **1978**, *97*, 148.

(9) (a) Ayalon-Chass, D.; Ehlinger, E.; Magnus, P. *J. Chem. Soc., Chem. Commun.* **1977**, 722. (b) Ehlinger, E.; Magnus, P.; *Tetrahedron Lett.* **1980**, 11. (c) Ehlinger, E.; Magnus, P. *J. Am. Chem. Soc.* **1980**, *102*, 5004.

(10) (a) Amouroux, R.; Chan, T. H. *Tetrahedron Lett.* **1978**, 4453. (b) Lau, P. W. K.; Chan, T. H. *Tetrahedron Lett.* **1978**, 2383.

(11) Fraenkel, G.; Chow, A.; Winchester, W. R. *J. Am. Chem. Soc.* **1990**, *112*, 2582–2585.

(12) Fraenkel, G.; Chow, A.; Winchester, W. R. *J. Am. Chem. Soc.* **1990**, *112*, 1382–1386.

(13) Fraenkel, G.; Winchester, W. R. *Organometallics* **1990**, *9*, 1314–1316.

(14) Boche, G.; Fraenkel, G.; Cabral, J.; Harms, K.; van Eikama-Hommes, W. J. R.; Lohrenz, J.; Marsch, M.; Schleyer, P. v. R. *J. Am. Chem. Soc.* **1992**, *114*, 1562–1565.

(15) Fraenkel, G.; Cabral, J. *J. Am. Chem. Soc.* **1992**, *114*, 9067–9075.

(16) (a) Horvath, R. F.; Chan, T. H. *J. Org. Chem.* **1989**, *54*, 319. (b) Chan, T. H.; Koumaglo, K.; Horvath, R.; Wang, D.; Wei, Z.; Yi, G. L.; Li, J. S. *Silicon Chemistry*; Corey, E. R., Corey, J. Y., Gaspar, P. P., Ed.; Ellis-Harwood: Chester, 1988; Chapter 5, p 49.

0002-7863/93/1515-1551$04.00/0 © 1993 American Chemical Society

Table I. Proton NMR 4-exo and 4-endo Shifts and Coupling Constants (J)

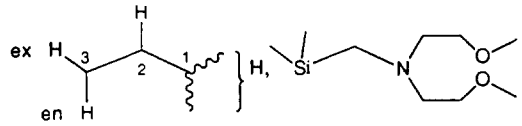

	THF-d_8[a]		toluene-d_8[b]	
	33% exo	67% endo	88% exo	12% endo
		Shifts, δ		
C_1H	1.39	1.57	2.57	
C_2H	6.09	6.50	6.86	7.45
C_3H_{ex}	2.58	2.58	3.52	
C_3H_{en}	2.82	2.82	3.80	
$SiCH_3$	−0.16	−0.08, −0.10	0.31	0.44
$SiCH_2$	1.79	1.79	1.69	
NCH_2C	2.35, 2.07	2.35, 2.47	2.77	
OCH_2	3.57	3.57	3.15	
OCH_3	3.32	3.29, 3.26	2.97	
		J, Hz		
C_1H, C_2H	15.16	11.01	15.32	11.81
C_2H, C_3H_{ex}	8.89	9.59	8.32	9.92
C_2H, C_3H_{en}	15.16	16.26	15.32	15.86

[a] 200 K. [b] 240 K.

Below, we report NMR studies of **4** which confirm the proposal for a folded structure and reveal the intimate details of its internal dynamic behavior, of relative motions inside *ion pairs*.

Results and Discussion

Compound **5** was treated with *n*-butyllithium in pentane–diethyl ether at −92 °C for 1.5 h. The resulting precipitate was washed with diethyl ether, dried in vacuo (−78 °C to room temperature), and then stored under an argon atmosphere until used. Samples for NMR study were dissolved in toluene-d_8 and in THF-d_8.

We previously reported the predilection of trimethylsilyl substituents at the termini of allyllithium to occupy exo sites, as observed for **1–3**, in all media tried and at least within the temperature range 160–320 K.[11-13] In contrast, NMR of **4** at low temperature reveals the existence of two isomers, **4**-exo and **4**-endo, as evidenced from proton NMR of the allyl moieties, Table I. There are two clearly resolved C_2H multiplets: one incorporating the larger vicinal C_1H–C_2H coupling of 15.16 Hz indicating the *exo*-silyl species; the other, 11.01 Hz for **4**-endo; Figure 1. The two species show different shifts for C_1H, $SiCH_3$, and OCH_3 in proton NMR, as well as among the ^{13}C resonances for C_2, CH_3Si, CH_2Si, CH_2N, CH_2O, and CH_3O; see Tables I and II.

The **4**-exo/**4**-endo ratio is different in the two media investigated, being 0.49 in THF-d_8 and 7.3 in toluene-d_8; see Figure 1. From NMR data obtained between 160 and 320 K, these ratios appear to change very little, less than 3%.

Further nonequivalencies observed at low temperature among the proton and ^{13}C resonances of **4**-endo and **4**-exo support the folded structures proposed by Chan and Horvath.[16] For example, at 160 K the species assigned to **4**-endo in THF exhibited *equal doublets* for $SiCH_3$, NCH_2, and OCH_3 in proton NMR and for CH_2N, CH_2O, and CH_3O in ^{13}C NMR; see Table II. These effects are not seen for **4**-exo in THF. In toluene-d_8 the situation for **4**-exo is reversed, with equal doublets in ^{13}C NMR for CH_3Si, CH_2N, CH_2O, and CH_3O. The **4**-endo species in toluene-d_8 was too dilute to provide useful NMR data. All the ^{13}C NMR data for **4**-exo and **4**-endo, obtained at low temperature, are listed in Table II.

Since the ^{13}C chemical shifts in the pendant ligand in **4**-exo and **4**-endo are quite different from those for starting material, we can assume that all sites, oxygens and nitrogen, are coordinated to lithium. This, together with the observation of magnetically nonequivalent CCH_2N, OCH_3, and OCH_2 ^{13}C's within the complex, strongly supports the folded structure; see **4**. Such a structure maximizes electrostatic attraction between Li^+ and allyl anion. However, these results do not rule out a head-to-tail dimer.

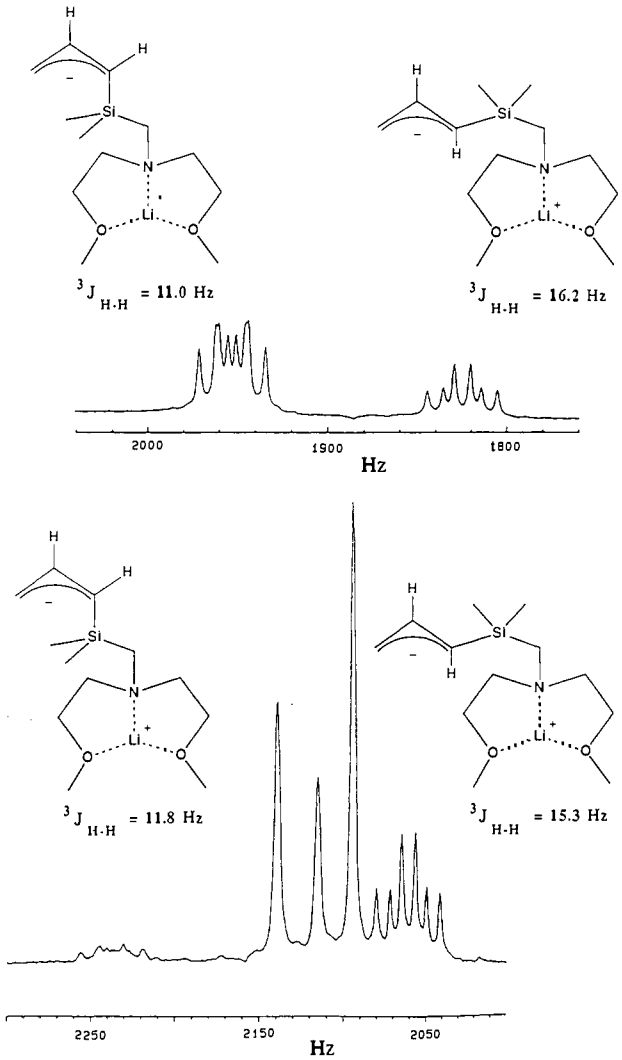

Figure 1. Proton NMR, 300 MHz, C_2H of **4**-exo and **4**-endo in THF-d_8 at 200 K (top) and in toluene-d_8 at 240 K (bottom).

Table II. ^{13}C NMR **4**-exo[a] and **4**-endo[a] Shifts, δ

	THF-d_8[b]		toluene-d_8[c]	
	exo	endo	exo	endo
C_1	45.09	45.09	50.66	
C_2	146.61	148.12	147.55	
C_3	74.48	74.48	66.30	
CH_3Si	1.26	−3.14	1.60	
			1.33	
CH_2Si	43.60	42.31	48.93	
CH_2CN	55.57	53.39, 56.95	48.93, 53.10	
CH_2O	69.35	69.15, 68.79	69.68, 68.33	
CH_3O	59.58	59.01, 58.97	59.10, 59.20	

[a] See heading of Table I. [b] 200 K. [c] 240 K.

With increasing temperature two kinds of signal averaging are observed in NMR spectra of **4** in THF-d_8 and toluene-d_8. Between 245 and 315 K there is progressive averaging of resonances of **4**-exo with **4**-endo, as, for example, among the data for C_2H proton resonances; see Figure 2. This is clearly the result of rotation around the C_1–C_2 allyl bond (eq 1). The coalescence is also seen in the ^{13}C NMR line shapes for sites on the pendant ligand, e.g., OCH_2 and NCH_2C. A second, faster process detected among the ^{13}C NMR data from 210 to 250 K is responsible for averaging of shifts *within* one of the **4**-exo or **4**-endo species. For example, with increasing temperature, the equal doublets in ^{13}C NMR due to CCH_2N and OCH_2 in **4**-exo in toluene-d_8 progressively average to single lines at their respective centers, as shown in Figures 3 and 4. It will be shown that a common mechanism is responsible for these latter line-shape changes. Phenomenologically this must

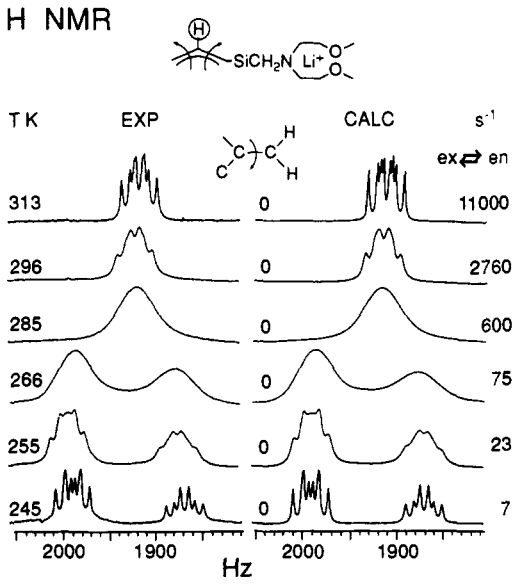

Figure 2. (Left) Proton NMR, 300 MHz, C_2H of **4**-exo and **4**-endo in THF-d_8 at different temperatures. (Right) Calculated line shapes with exo–endo interconversion rate constants.

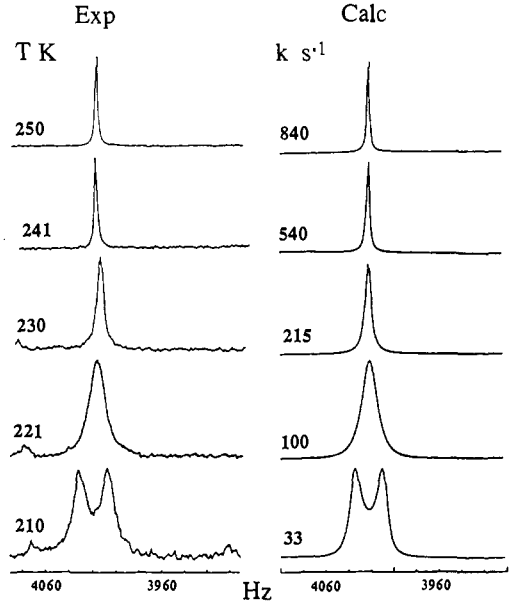

Figure 3. ^{13}C NMR line shapes, 75.4 MHz, CCH_2N of **4**-exo in toluene-d_8. (Left) Experimental spectra, different temperatures. (Right) Calculated spectra with rate constants for exo–exo reorientation.

be due to inversion at lithium, i.e., the overall process shown in eq 2. For the moment, this is ascribed to rotation of bound ligand around the Si–C_1 (allyl) bond.

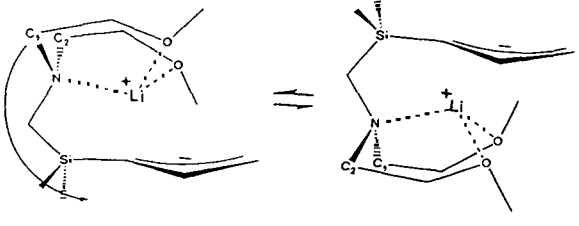

(2)

In the case of **4** in THF-d_8, both **4**-exo and **4**-endo are abundant. All ^{13}C sites on the pendant ligand in **4**-endo are magnetically nonequivalent, while in **4**-exo there is one single peak each for OCH_2, OCH_3, and NCH_2C; see Table II. The line-shape changes, e.g., for OCH_2, are due to both processes already proposed above; see Figure 5. Within the lower temperature range, 195–240 K, there is averaging of the nonequivalent OCH_2 resonances of **4**-endo, while above 240 K with increasing temperature all OCH_2 resonances for both species average to a single line, by 296 K.

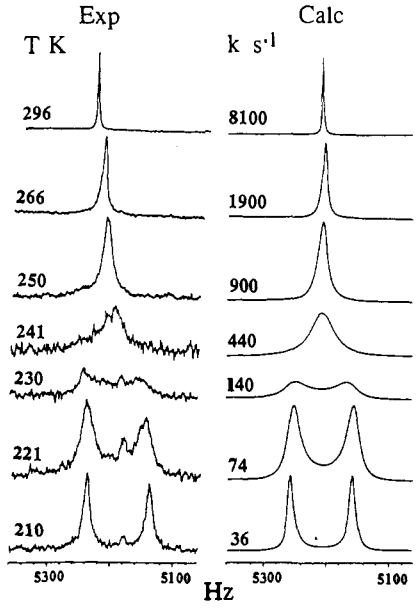

Figure 4. ^{13}C NMR line shapes, 75.4 MHz, OCH_2 of **4**-exo in toluene-d_8. (Left) Experimental spectra, different temperatures. (Right) Calculated spectra with rate constants for exo–exo′ reorientation.

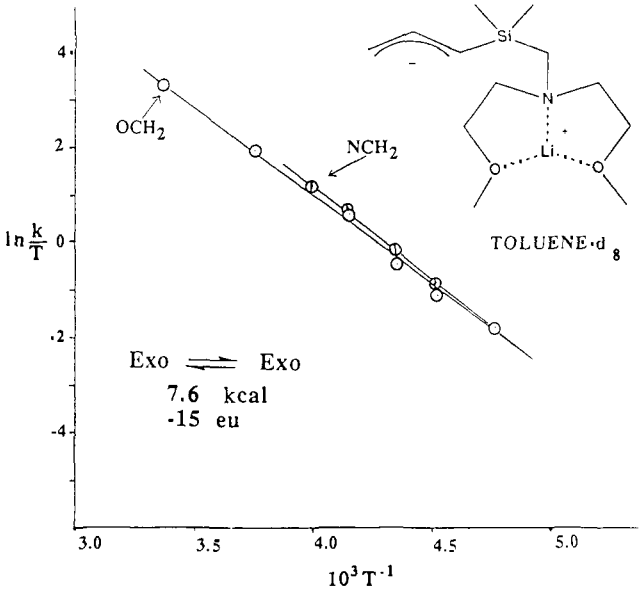

Figure 5. Eyring plots for exo–exo reorientation in **4**-exo in toluene-d_8 using OCH_2 and CCH_2N ^{13}C NMR line shapes.

The NMR line shapes in proton-decoupled ^{13}C NMR perturbed by conformational dynamics are treated as uncoupled multi half spin exchanging systems.[17,18] Thus, line-shape analysis of the coalescence and signal averaging of the equal doublets in ^{13}C NMR of **4**-exo in toluene-d_8 due to NCH_2C and OCH_2 give the calculated absorptions shown on the right sides of Figures 3 and 4, respectively. The resulting Eyring plots, Figure 5, give essentially the same activation parameters for both sets of line shapes, $\Delta H^{\ddagger} = 7.6$ kcal/mol and $\Delta S^{\ddagger} = -15$ eu.

Analysis of the OCH_2 ^{13}C line shapes from the equilibrium mixture **4**-exo with **4**-endo in THF-d_8, Figure 6, is more complicated than the previous case since two species are present and two dynamic processes are responsible for changes in the line

(17) (a) Gutowsky, H. S.; Saika, H. *J. Chem. Phys.* **1953**, *21*, 1688. (b) Gutowsky, H. S.; Holm, C. H. *Ibid.* **1957**, *25*, 1288.

(18) (a) McConnell, H. M.; Holm, C. H. *J. Chem. Phys.* **1958**, *28*, 430. (b) Anderson, P. W. *J. Phys. Soc. Jpn* **1954**, *9*, 316. (c) Sack, R. A. *Mol. Phys.* **1958**, *1*, 163.

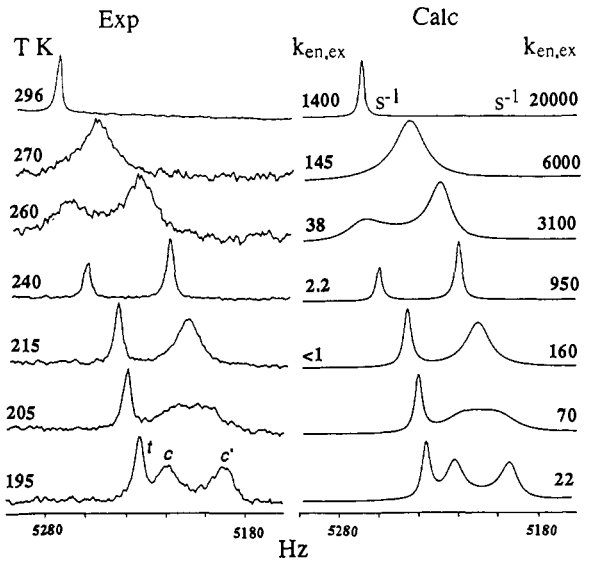

Figure 6. ^{13}C NMR line shapes, OCH_2 of **4**-exo and **4**-endo in THF-d_8. (Left) Experimental spectra, different temperatures. (Right) Calculated spectra with rate constants for exo–endo′ interconversions.

shapes.[19] The single line labeled t is due to **4**-exo, and the equal doublet, c and c′, comes from **4**-endo; see Figure 6. This system exhibits three-site exchange, the averaging of c with t and of c′ with t due to rotation around the C_1–C_2 (allyl) bond (eq 3),

$$\mathbf{c} \underset{k_{tc}}{\overset{k_{ct}}{\rightleftharpoons}} \mathbf{t} \tag{3}$$

$$\frac{k_{ct}}{k_{tc}} = K \tag{4}$$

together with the faster proposed rotation of complexed pendant ligand around the Si–C (allyl) bond which averages c with c′ (eq 5). To calculate line shapes for this system requires solving for

$$\mathbf{c} \overset{k_{cc'}}{\rightleftharpoons} \mathbf{c}' \tag{5}$$

the three elements of the density matrix for c and t given as $\langle\alpha|\rho^c|\beta\rangle$, $\langle\alpha|\rho^{c'}|\beta\rangle$, and $\langle\alpha|\rho^t|\beta\rangle$, the two states in each element being connected by a $\Delta m = +1$ transition;[17,18] for brevity these elements will be rewritten as ρ^c, $\rho^{c'}$, and ρ^t, respectively. The contribution of the two exchange processes to the density matrix equations is given by eqs 6–8, where E is the exchange operator.[19]

$$E\rho^t = k_{tc}(\rho^c + \rho^{c'} - 2\rho^t) \tag{6}$$

$$E\rho^c = k_{ct}(\rho^t - \rho^c) + k_{cc'}(\rho^{c'} - \rho^c) \tag{7}$$

$$E\rho^{c'} = k_{ct}(\rho^t - \rho^{c'}) + k_{cc'}(\rho^c - \rho^{c'}) \tag{8}$$

Then solving the derived coupled density matrix equations shown in matrix form in eq 9 gives the ρ elements. In eq 9 ν_i values are

$$\begin{bmatrix} i2\pi(\nu-\nu_c)-\frac{1}{T} & -k_{ct}-k_{cc} & k_{cc} & k_{ct} \\ k_{cc} & i2\pi(\nu-\nu_c)-\frac{1}{T} & -k_{ct}-k_{cc} & k_{ct} \\ k_{tc} & k_{tc} & i2\pi(\nu-\nu_t)-\frac{1}{T} & -2k_{tc} \end{bmatrix} \times \begin{bmatrix} \rho^c \\ \rho^c \\ \rho^t \end{bmatrix} = iC \begin{bmatrix} 1 \\ 1 \\ 1 \end{bmatrix} \tag{9}$$

shifts, $1/T$ is the natural line width, and C is a constant. Finally, the ρ elements are summed and weighted with the appropriate

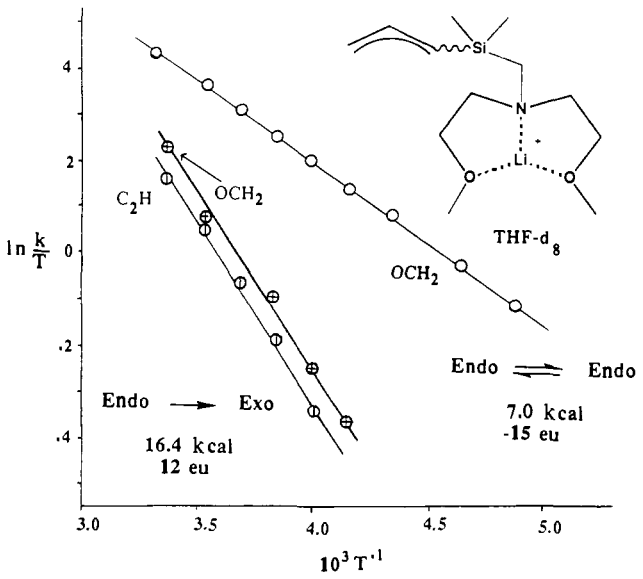

Figure 7. Eyring plots for rotation around C_1–C_2, endo–exo, and around Si–C_1 (allyl) in the equilibrium mixture of **4**-exo with **4**-endo in THF-d_8, using different ^{13}C NMR line shapes.

Table III. Activation Parameters for Rotation in **4**-endo and **4**-exo[a]

	resonance	$\Delta H^\ddagger$ (kcal/mol)	$\Delta S^\ddagger$ (eu)	$\Delta G^\ddagger$ (298 K) (kcal/mol)
		In THF-d_8		
endo → exo	OCH_2	16.4	11.7	12.9
endo → exo	C_2H	15.4	9.2	12.6
endo → exo	C_2H	7.0	12.3	12.7
endo → endo	OCH_2	16.4	−15.0	11.5
		In Toluene-d_8		
exo → exo	OCH_2	7.6	−15.0	12.0
exo → exo	NCH_2	8.1	−12.0	11.7

[a] Rotation around allyl C_1–C_2, endo → exo; rotation around Si–Cl_1.

concentration factors, t and c, to yield the calculated absorption, Abs(ν) (eq 10). Comparison of experimental with calculated

$$\mathrm{Abs}(\nu) = -\mathrm{Im}\left[t\rho^t + \left(\frac{c}{2}\right)\rho^c + \left(\frac{c}{2}\right)\rho^{c'}\right] \tag{10}$$

fitted line shapes, Figure 6, yields the two sets of rate constants k_{ct} and $k_{cc'}$. The resulting Eyring plots, Figure 7, give the activation parameters for rotation around Si–C (allyl) and C_1–C_2 which are listed in Table III.

The barrier to rotation around C_1–C_2 in **4** in THF-d_8 was determined separately from the ^{13}C line shape of C_2 (allyl), Table III, as well as by using the C_2H proton NMR.[14] These line shapes were also used to estimate the rates of rotation around the C_2–C_3 (allyl) bond. For convenience, we renumber the hydrogens as shown in Figure 8. Since the H_3 resonance is well resolved from the other allylic proton resonances, one need only solve for the first-order transitions of H_3. The required elements of the density matrix of t or c using the spin-product representation are written as in eq 11, where the order of spins follows the numbering in

$$\langle a_1b_2\alpha_3c_4|\rho^{t(c)}|a_1b_2\beta_3c_4\rangle \equiv \rho^{t(c)}_{ab\alpha c,ab\beta c} \tag{11}$$

the diagrams, Figure 8. These elements are off-diagonal in spin functions of H_3 ($\Delta M = 1$) and diagonal in the spin product for H_1, H_2, and H_4. Eight such elements are written each for **4**-exo(t) and **4**-endo(c). Given solutions for the 16 coupled density matrix equations, the absorption is obtained from the imaginary part of the sum in eq 12 suitably weighted with concentration factors.

$$\mathrm{Abs}(\nu) = -\mathrm{Im}\left(t\sum_{1}^{8}\rho^t_{l,m} + c\sum_{9}^{16}\rho^c_{l,m}\right) \tag{12}$$

(19) (a) Kaplan, J. I.; Fraenkel, G. *J. Am. Chem. Soc.* **1972**, *94*, 2907. Kaplan, J. I.; Fraenkel, G. *NMR of Chemically Exchanging Systems*; Academic Press: New York, 1980; Chapter 6.

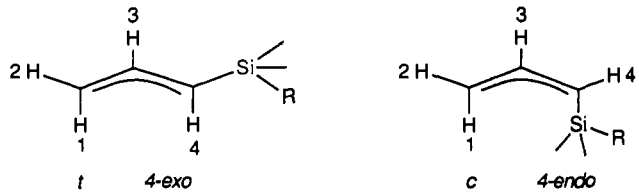

Figure 8. Numbering of allyl hydrogens in **4**-exo and **4**-endo for purposes of proton NMR line shape analysis.

The 16 elements of the density matrix equation take the form

$$\left[i[\rho^t,H^t] - \frac{\rho^t}{T} + k^t_{tc}[\rho^t(a1) - \rho^t] + k^t_2[\rho^t(a2) - \rho^t] \right]_{l,m} = 0 \quad (13)$$

where k_{tc} and k_2 are first-order rate constants for rotation around C_1–C_2 and C_2–C_3, respectively, in **4**-exo/**4**-endo and *a*1 or *a*2 labels the density matrix after a rotation around C_1–C_2 or C_2–C_3 bond, respectively. Note that these last two terms take account of the effects of exchange, including their mechanisms, on the NMR line shapes. In a second set of equations, *t* is switched with *c*. Since the two H_3 resonances are first order, the Hamiltonian in radians/second in the rotating frame (for t) is given by eq 14. Terms

$$H^t = 2\pi(\nu^t_3 - \nu)I^z_3 + 2\pi\psi_3 I^x_3 + 2\pi(J^t_{1,3}I^z_1I^z_3 + J^t_{2,3}I^z_2I^z_3 + J^t_{3,4}I^z_3I^z_4) \quad (14)$$

for the other allyl hydrogens are not included since we only need to plot the H_3 absorption. Elements of the commutator take the form

$$i(H^t_{m,m} - H^t_{l,l})\rho^t_{l,m} + k_{tc}[\rho^t(a1) - \rho^t]_{l,m} - k_2[\rho^t(a2) - \rho^t]_{l,m} - \frac{\rho_{l,m}}{T} = -iC \quad (15)$$

where *C* is a constant. It remains to determine elements of the density matrix after exchange. Rotation around C_2–C_3 exchanges the sites of H_1 and H_2 so that

$$\rho(a2)^{t(c)}_{ab\alpha c,ab\beta c} = \rho^{t(c)}_{ba\alpha c,ba\beta c} \quad (16)$$

while rotation about C_1–C_2 leaves the order of spin functions unchanged but changes the label of ρ (eq 17). The resulting 16

$$\rho(a1)^{t(c)}_{ab\alpha c,ab\beta c} = \rho^{c(t)}_{ab\alpha c,ab\beta c} \quad (17)$$

coupled density matrix equations are solved for the $\rho^{t(c)}_{l,m}$ elements and the latter summed according to eq 12 to give the absorption; density matrix equations are listed in the Appendix. In Figure 2, right side, are displayed line shapes so calculated to fit the experimental spectra. The resulting Eyring plot is shown in Figure 9, giving $\Delta H^\ddagger$ = 16.4 kcal/mol. Interestingly, this analysis does not depend on the rate of rotation around C_2–C_3. It is apparently too slow to perturb the proton NMR line shape of H_3. In the case of **4** in toluene-d_8 solution, the endo isomer is too dilute to allow for an accurate determination of the C_1–C_2 barrier.

Altogether, the barrier to C_1–C_2 rotation has been measured from three sets of line shapes for **4** in THF-d_8, proton NMR of C_2H as well as ^{13}C data from OCH_2 and C_2H; with very similar results: see Table III. All the $\Delta H^\ddagger$ values lie within the range 16 ± 0.5 kcal/mol with $\Delta S^\ddagger$ = 10 ± 2 eu.

The second and faster of the two dynamic processes is detected from signal averaging in ^{13}C NMR of nonequivalent carbons on the pendant ligand in **4**-endo in THF-d_8 and in **4**-exo in toluene-d_8. *All* these analyses lead to very similar activation parameters, $\Delta H^\ddagger$ = 7 kcal/mol and $\Delta S^\ddagger$ = −11 to −15 eu, clearly the result of a common process. Experiments carried out using different concentrations of **4** in THF gave rise to very similar line shapes. This argues that the two dynamic processes are first order in **4** or some aggregate thereof. The simplest and most attractive mechanism for the faster process is that it comes from rotation of coordinated lithium around the C_1–Si bond. One can imagine other mechanisms, for example, involving ligand–lithium dissociation. Although these cannot all be ruled out, the results presented above strongly favor the rotational mechanism.

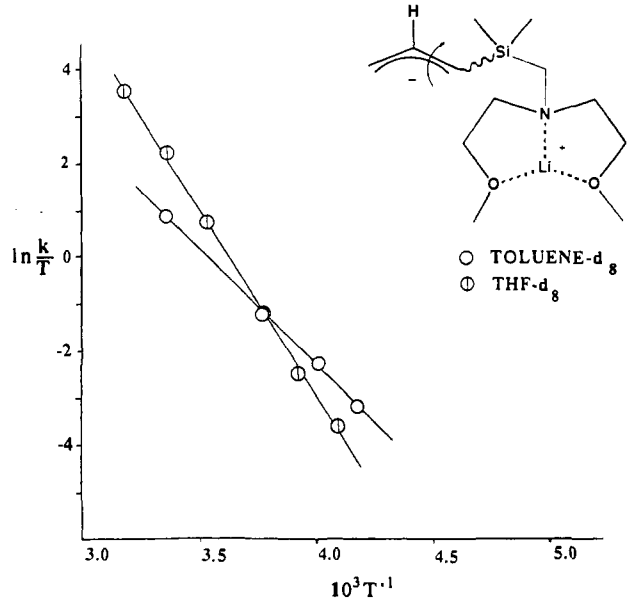

Figure 9. Eyring plots for rotation around C_1–C_2 (allyl) in **4**-exo and **4**-endo in THF-d_8 and toluene-d_8.

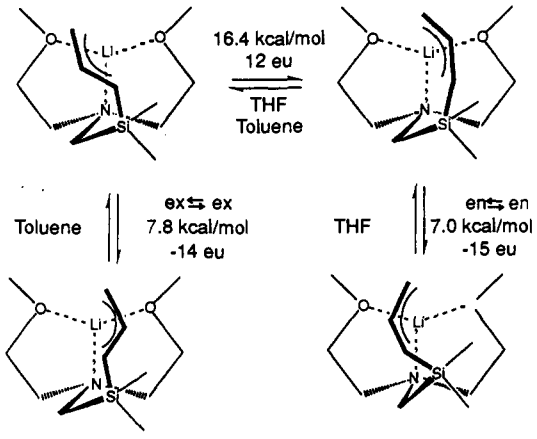

Figure 10. Summary of activation parameters for reorientation of ions within **4**-exo and **4**-endo.

As noted in the introduction, effects similar to those seen for **4** have also been observed in NMR studies of TMEDA complexed to *exo,exo*-[1,3-bis(trimethylsilyl)allyl]lithium,[12] pentamethyldiethylenetriamine complexed to [1-(trimethylsilyl)allyl]lithium,[11] and the TMEDA complex of (1,1,3,3-tetramethylallyl)lithium.[15] All these species exhibited nonequivalence among carbons on the complexed ligand, carbons which would be equivalent in the free ligand. In each case, the analysis of signal averaging of these resonances leads to activation enthalpies of 7–8 kcal/mol. Hence, we ascribed all these effects to reorientation of complexed Li^+ with respect to counterion. In the case of **4**, with the ligand attached to silicon, this reorientation motion is constrained to the rotation around the Si–C_1 bond of coordinated lithium, with a $\Delta H^\ddagger$ value of 7–8 kcal/mol. These results are summarized in Figure 10.

These studies also show that while rates of rotation around the C_1–C_2 bond in **4** lie on the NMR time scale and are easily measured using NMR line-shape analysis, rotation around the C_2–C_3 bond is too slow to measure up to 318 K. The rate constant at this temperature for rotation about the equivalent bond in *exo*-[1-(trimethylsilyl)allyl]lithium in THF is 349 s^{-1}.[11]

In cases where the effect has been investigated, it has been found that barriers to rotation in allyllithiums depend significantly on the nature of the lithium ligand present.[11] It has been proposed that the transition state for rotation involves some increase in

covalence between lithium and one terminal carbon on allyl, or at least a tighter type of ion pairing compared to the ground state.[3,11] Models of **4** in which lithium is complexed tridentately or bidentately show lithium to be sited near C_1 and C_2, not C_3. Thus, lithium is not close enough to C_3 for covalency or a tighter ion pair to develop.

Conclusions

In sum, we have shown that a (1-silylallyl)lithium with a pendant ligand attached to silicon, **4**, consists of a mixture of 1-endo and 1-exo species. In contrast, other terminal (silylallyl)lithiums take the exo structures exclusively. NMR shows that compounds **4**-exo and **4**-endo assume the folded structures; see **4**. New insight into the structure and the dynamic behavior of these ion pairs shows reorientation of the two ions relative to each other *within* the ion pair to be quite slow, with a barrier of 7–8 kcal/mol depending on the medium. Whereas this effect has been detected before with similar activation parameters, in the case of **4**-exo and **4**-endo the ion reorientation process is the result of rotation of bound Li^+ around the Si–C_1 (allyl) bond.

Experimental Section

[1-[[[Bis(2-methoxyethyl)amino]methyl]dimethylsilyl]allyl]lithium (4). A 50-mL Schlenk flask containing a glass-coated stir bar was flamed and cooled under vacuum and then charged with *n*-butyllithium in pentane (0.37 mL, 0.11 mmol, 0.3 M) under argon. The flask was brought to −92 °C with an external bath, and the reagent was then diluted with 1.2 mL of dry diethyl ether. To this was added dropwise from a syringe allyl[bis(2-methoxyethyl)amino]methyl]dimethylsilane (0.05 mL, 0.155 mmol).[1] Within minutes the solution became cloudy, and compound **4** began to precipitate. After 1.5 h at −92 °C stirring was stopped, and the precipitate was allowed to settle. The reaction solvent was then removed with a syringe and replaced with 2 mL of fresh diethyl ether introduced slowly and cold by running the solvent down the side of the reaction flask. The mixture was then stirred for 5 min, and the organolithium compound was again allowed to settle. The solvent was then removed and replaced with fresh ether as described above; after the mixture was stirred for 15 min, the above procedure was repeated once more. The flask of the washed allyllithium was then vacuum dried initially at −78 °C to remove diethyl ether. The flask was then allowed to come to room temperature and was then transferred to a glovebox. A sample of the solid organolithium compound was then placed in a NMR tube fitted with a vacuum adaptor, which was removed from the glovebox and connected to a high-vacuum line. The dried allyllithium compound was dissolved with vacuum-transferred deuterated THF or toluene. ^{1}H NMR (THF, ppm, 318 K): OCH_2 3.258 (t, $^3J(OCH_2–NCH_2)$ = 5.33 Hz), NCH_2 2.432 (t), $Si(CH_3)_2$ −0.31 (s), $SiCH_2$ 1.680 (s), OCH_3 3.12 (s), allyl $C3H_2$ 2.830 and 2.519 (m, ^3J(C2H–C3H) = 15.63 Hz, ^2J(C3H–C3H′) = 2.71 Hz, ^3J(C2H–C3H) = 8.915 Hz), C1*H* 1.438 (d, ^3J(C2H–C1H) = 13.66 Hz), C2*H* 6.152 (m). ^{13}C NMR (THF, ppm, 296 K): *C*1H 47.04, *C*2H 147.74, $C3H_2$ 72.40, $Si(CH_3)_2$ − 0.27, $SiCH_2$ 44.43, NCH_2 56.06, OCH_2 69.96, OCH_3 59.30. NMR samples of **4** for line-shape analyses were 0.23 M (0.032 g) in 0.6 mL of THF-d_8 and 0.41 M (0.062 g) in 0.6 mL of toluene-d_8; results of dynamics in THF were the same at 0.94 M.

Acknowledgment. This research was generously supported by the National Science Foundation, Grant No. CHE8304636. NMR equipment used in this research was financed in part with grants from the National Science Foundation to the Chemistry Department. Dr. Charles Cottrell, Central Campus Instrumentation Center, The Ohio State University, provided invaluable technical advice. We also are pleased to acknowledge valuable discussions with Dr. R. William Winchester, Trinity University, San Antonio, who initiated work on the problem. Professor T. Chan, McGill University, generously supplied the starting material used in this work.

Appendix

NMR Line-Shape Analysis of the Proton Line Shape of H_3 in 4-exo and 4-endo. The density matrix equation in matrix form is

$$\mathbf{A}\rho_{col} = i\mathbf{C}\mathbf{B}_{col} \quad (A1)$$

in which the $\rho_{l,m}$ elements of ρ_{col} are in numerical order, ρ_1 to ρ_{16}, and all $b_i = 1$.

The 16 elements of the density matrix, $\rho_{l,m}$, where l and m are states connected by a $\Delta m = +1$ proton transition of H_3 in **4**-exo(t) and **4**-endo(c), are listed:

ρ	m	index $\rho^t_{l,m}$	index $\rho^c_{l,m}$
αααα	ααβα	1	9
βααα	βαβα	2	10
αβαα	αββα	3	11
αααβ	ααββ	4	12
ββαα	βββα	5	13
βααβ	βαββ	6	14
αβαβ	αβββ	7	15
ββαβ	βββββ	8	16

Elements of the 16 × 16 coefficient matrix **A** are listed below.

$$a_{1,1} = i2\pi\Delta\nu_t - \frac{1}{T} - k_{tr} - k_{tc} + i\pi(-J^t_{1,3} - J^t_{2,3} - J^t_{3,4}) \quad (A2)$$

$$a_{2,2} = i2\pi\Delta\nu_t - \frac{1}{T} - k_{tr} - k_{tc} + i\pi(J^t_{1,3} - J^t_{2,3} - J^t_{3,4}) \quad (A3)$$

$$a_{3,3} = i2\pi\Delta\nu_t - \frac{1}{T} - k_{tr} - k_{tc} + i\pi(-J^t_{1,3} + J^t_{2,3} - J^t_{3,4}) \quad (A4)$$

$$a_{4,4} = i2\pi\Delta\nu_t - \frac{1}{T} - k_{tc} + i\pi(-J^t_{1,3} - J^t_{2,3} + J^t_{3,4}) \quad (A5)$$

$$a_{5,5} = i2\pi\Delta\nu_t - \frac{1}{T} - k_{tc} + i\pi(J^t_{1,3} + J^t_{2,3} - J^t_{3,4}) \quad (A6)$$

$$a_{6,6} = i2\pi\Delta\nu_t - \frac{1}{T} - k_{tr} - k_{tc} + i\pi(J^t_{1,3} - J^t_{2,3} + J^t_{3,4}) \quad (A7)$$

$$a_{7,7} = i2\pi\Delta\nu_t - \frac{1}{T} - k_{tr} - k_{tc} + i\pi(-J^t_{1,3} + J^t_{2,3} + J^t_{3,4}) \quad (A8)$$

$$a_{8,8} = i2\pi\Delta\nu_t - \frac{1}{T} - k_{tc} + i\pi(J^t_{1,3} + J^t_{2,3} + J^t_{3,4}) \quad (A9)$$

$$a_{9,9} = i2\pi\Delta\nu_c - \frac{1}{T} - k_{tc} + i\pi(-J^c_{1,3} - J^c_{2,3} - J^c_{3,4}) \quad (A10)$$

$$a_{10,10} = i2\pi\Delta\nu_c - \frac{1}{T} - k_{ct} - k_{cr} + i\pi(J^c_{1,3} - J^c_{2,3} - J^c_{3,4}) \quad (A11)$$

$$a_{11,11} = i2\pi\Delta\nu_c - \frac{1}{T} - k_{ct} - k_{cr} + i\pi(-J^c_{1,3} + J^c_{2,3} - J^c_{3,4}) \quad (A12)$$

$$a_{12,12} = i2\pi\Delta\nu_c - \frac{1}{T} - k_{ct} + i\pi(-J^c_{1,3} - J^c_{2,3} + J^c_{3,4}) \quad (A13)$$

$$a_{13,13} = i2\pi\Delta\nu_c - \frac{1}{T} - k_{ct} + i\pi(J^c_{1,3} + J^c_{2,3} - J^c_{3,4}) \quad (A14)$$

$$a_{14,14} = i2\pi\Delta\nu_c - \frac{1}{T} - k_{ct} - k_{cr} + i\pi(J^c_{1,3} - J^c_{2,3} + J^c_{3,4}) \quad (A15)$$

$$a_{15,15} = i2\pi\Delta\nu_c - \frac{1}{T} - k_{ct} - k_{cr} + i\pi(-J^c_{1,3} + J^c_{2,3} + J^c_{3,4}) \quad (A16)$$

$$a_{16,16} = i2\pi\Delta\nu_c - \frac{1}{T} - k_{ct} + i\pi(J^c_{1,3} + J^c_{2,3} + J^c_{3,4}) \quad (A17)$$

$$a_{1,9} = k_{tc} \quad (A18)$$

$$a_{2,3} = k_{tr} \quad (A19)$$

$$a_{2,10} = k_{tc} \quad (A20)$$

$$a_{3,2} = k_{tr} \quad (A21)$$

$$a_{3,11} = k_{tc} \quad (A22)$$

$$a_{4,12} = k_{tc} \quad (A23)$$

$$a_{5,13} = k_{tc} \quad (A24)$$

$$a_{6,7} = k_{tr} \quad (A25)$$

$$a_{6,14} = k_{tc} \quad (A26)$$

$$a_{7,6} = k_{tr} \quad (A27)$$

$$a_{7,15} = k_{tc} \quad (A28)$$

$$a_{8,15} = k_{tc} \quad (A29)$$

$$a_{9,1} = k_{ct} \quad (A30)$$

$$a_{10,2} = k_{ct} \quad (A31)$$

$$a_{10,11} = k_{cr} \quad (A32)$$

$$a_{11,3} = k_{ct} \quad (A33)$$

$$a_{11,10} = k_{cr} \quad (A34)$$

$$a_{12,4} = k_{ct} \quad (A35)$$

$$a_{13,5} = k_{ct} \quad (A36)$$

$$a_{14,6} = k_{ct} \quad (A37)$$

$$a_{14,15} = k_{cr} \quad (A38)$$

$$a_{15,7} = k_{ct} \quad (A39)$$

$$a_{15,14} = k_{cr} \quad (A40)$$

$$a_{10,8} = k_{ct} \quad (A41)$$

Solution of the coupled density matrix equations provides the elements $\rho_i^{c(t)}$, which are summed with concentration weighting to give the absorption.

$$\mathrm{Abs}(\nu) = -\mathrm{Im}(c\sum_{i=8}^{16}\rho_i^c + t\sum_{i=1}^{8}\rho_i^t) \quad (A42)$$

Rearrangement Mechanisms of $B_{12}H_{12}^{2-}$ and $C_2B_{10}H_{12}$

David J. Wales

Contribution from the University Chemical Laboratories, Lensfield Road, Cambridge CB2 1EW, UK. *Received July 24, 1992*

Abstract: Rearrangement mechanisms for $B_{12}H_{12}^{2-}$ and $C_2B_{10}H_{12}$ are deduced by ab initio calculations at the minimal basis set level. In contrast to most previous discussions, but in accord with orbital symmetry considerations, all the transition states are found to have low symmetry; the three carborane isomers of icosahedral $B_{12}H_{12}^{2-}$ interconvert via a complex series of higher energy minima. The results illustrate how these systems adapt to the lack of low-energy orbital-symmetry-allowed pathways and show that the topology of the potential energy surface changes significantly from the borane to the carborane.

Introduction

Speculations about how borane and carborane clusters rearrange have figured in the literature for several decades. The development of powerful orbital symmetry selection rules by the author and co-workers has recently enabled the relative rearrangement rates of these species to be explained, at least qualitatively.[1-4] Two fundamental cluster rearrangement mechanisms have also been characterized by detailed ab initio calculations including the effects of polarization basis functions and electron correlation.[5] One tantalizing problem, in particular, remains to be properly answered, namely the nature of the high-energy rearrangements of icosahedral $B_{12}H_{12}^{2-}$ and the associated carboranes $C_2B_{10}H_{12}$. The earliest work considered various high-symmetry processes, and this pattern has continued in the recent literature,[6] notwithstanding calculations which showed that the highest symmetry structures may be discounted as possible transition states.[1] Orbital symmetry considerations also suggested that lower symmetry, possibly multistep, processes might be involved,[1-3] given that no low-energy orbital-symmetry-allowed mechanisms are available. In this paper the potential energy surfaces of both $B_{12}H_{12}^{2-}$ and $C_2B_{10}H_{12}$ are investigated by ab initio calculations at the minimum basis set level, and numerous reaction pathways are characterized. Hence, this work also provides a detailed investigation of how an inorganic cluster may circumvent the lack of any low-energy orbital-symmetry-allowed pathways. Two key points emerge: (1) The topology of the $C_2B_{10}H_{12}$ potential energy surface is significantly different from that of $B_{12}H_{12}^{2-}$, although there are obvious interrelations. (2) The three carborane isomers of icosahedral $B_{12}H_{12}^{2-}$ probably rearrange via a series of higher energy minima that are linked by generally low symmetry transition states. There are, however, some important caveats that must be established. First, the present results have been obtained from the SCF approximation with a minimal STO-3G basis. Second, the large number of higher energy minima and transition states obtained means that the investigation is incomplete and that the interconversion routes obtained may not be the lowest available. Third, some of the energy barriers involved are rather large, and it is conceivable that excited electronic states could also be involved.

The minimal basis set SCF approach was unavoidable in this study with current computational resources. Each search step required the calculation of analytic first and second derivatives

(1) Wales, D. J.; Stone, A. J. *Inorg. Chem.* **1987**, *26*, 3845.
(2) Wales, D. J.; Mingos, D. M. P.; Lin, Z. *Inorg. Chem.* **1989**, *28*, 2754.
(3) Wales, D. J.; Mingos, D. M. P. *Polyhedron* **1989**, *15*, 1933.
(4) Mingos, D. M. P.; Wales, D. J. *Introduction to Cluster Chemistry*; Prentice-Hall: Englewood Cliffs, 1990.
(5) Wales, D. J.; Bone, R. G. A. *J. Am. Chem. Soc.*, in press.
(6) Gimarc, B. M.; Warren, D. S.; Ott, J. J.; Brown, C. *Inorg. Chem.* **1991**, *30*, 1598.

0002-7863/93/1515-1557$04.00/0 © 1993 American Chemical Society